http://mmg.tversu.ru ISSN 2311-1275

MMG *Mathematical Modelling and Geometry*

Volume 3, No 1, p. 25 – 42 (2015)

ΛCDM vs multidimensional model in describing cosmological acceleration

G. S. Sharov and E. G. Vorontsova

Faculty of Mathematics, Tver State University, Sadovyi per. 35, Tver, Russia
e-mail: german.sharov@mail.ru

Received 13 January 2015. Published 27 January 2015.

Abstract. We consider observational manifestations of accelerated expansion of the Universe, in particular, recent data for type Ia supernovae, baryon acoustic oscillations and for the Hubble parameter $H(z)$ depending on redshift. We compare two models describing the mentioned observations: the ΛCDM model and the multidimensional model of I. Pahwa, D. Choudhury and T.R. Seshadri. For these models we calculate χ^2 functions for all measured effects, estimate optimal values of model parameters and their permissible errors.

Keywords: accelerated expansion, Hubble parameter, baryon acoustic oscillations, extra dimensions
MSC numbers: 83E15,83F05

1. Introduction

The accelerated expansion of our Universe is the most important discovery of last 20 years in astrophysics and explanation of this acceleration is the most urgent problem in modern cosmology. The first evidence of accelerated expansion resulted from Type Ia supernovae observations [1, 2].

Supernovae are stars which catastrophically explode with giant energy release and creation the expanding shell (the supernova remnant). All supernovae are divided into Type I with hydrogen-deficient optical spectrum and Type II with bright spectral hydrogen lines. The subdivision Type Ia in Type I is characterized by strong absorption near the silicon line 615 nm. Type Ia supernovae are believed to result from the thermonuclear ignition and disruption of carbon-oxygen white dwarfs while Type II come from core collapse of supergiant stars [3].

The peak luminosity of the supernova is up to 10^8 times brighter than before explosion, time dependence of the star's brightness (the light curve) gives possibility to estimate its absolute luminosity and to attribute this supernova to some class [3]. Type Ia supernovae have rather small dispersion among their peak absolute magnitudes, for these objects we can independently measure redshifts z and luminosity distances D_L, so Type Ia supernovae play a role of standard candles in the Universe.

Further observations of supernovae [4, 5], cosmic microwave background anisotropy [6], baryon acoustic oscillations [5, 7] and other observations [5, 6, 8] confirmed accelerated growth of the cosmological scale factor $a(t)$ at late stage of its evolution.

Baryon acoustic oscillations (BAO) are connected with propagation of acoustic waves in the relativistic plasma before the recombination epoch [5, 7]. These waves involved baryons coupled with photons up to the end of the drag era corresponding to $z_d \simeq 1059.3$ [8], then baryons became decoupled, the sound speed was abruptly decreased and the wave propagation was ended.

This effect may be observed as disturbances in the cosmic microwave angular power spectrum or as a peak in the correlation function of the galaxy distribution at the comoving sound horizon scale $r_s(z_d)$ [7, 8]. Observations of the BAO effect result in various manifestations [7] – [26], in particular, in estimations of the Hubble parameter $H(z)$ for different redshifts z [15] – [26] (details are in Sect. 2).

The mentioned recent observations of Type Ia supernovae, BAO effect and $H(z)$ estimates give stringent restrictions on possible cosmological theories and models. To satisfy these observational restrictions all models are to describe accelerated expansion of the Universe with definite parameters [27, 28].

The standard Einstein theory of gravitation predicts expansion of the Universe with deceleration corresponding $a''(t) < 0$. So to explain observed accelerated expansion, we are to modify the Einstein gravity. A lot of such modifications and alternative cosmological models have been suggested [27, 28]. The most simple modification is to use a Λ term (dark energy) resulting in cosmological solutions with acceleration. The corresponding model with cold dark matter in addition to deficient visible matter is now the most popular ΛCDM cosmological model (the Λ

term with cold dark matter) [27]. This model with appropriate parameters [5, 6, 8] successfully describes practically all observational data, in Sect. 3 we apply this model to describe the updated recent observations of Type Ia supernovae, BAO effects and $H(z)$ estimates.

One should note that there are some problems in the ΛCDM model, in particular, ambiguous nature of dark matter and dark energy, the problem of fine tuning for the observed value of Λ and the coincidence problem for surprising proximity Ω_Λ and Ω_m nowadays [27, 28].

Therefore cosmologists suggested many alternative models with nontrivial equations of state, with $f(R)$ Lagrangian, scalar fields, additional space dimensions and many others [27, 28, 29]. In particular, in Sect. 4 of this paper we consider in detail the multidimensional gravitational model of I. Pahwa, D. Choudhury and T.R. Seshadri [30] and the modified variant of this model [31, 32]. We compare predictions of these models and the ΛCDM model in describing recent data for Type Ia supernovae, BAO, $H(z)$ updated with respect to Ref. [32].

2. Observational data

The latest observational data on Type Ia supernovae were collected in the paper (and in the site) [4] after the Union2.1 satellite investigation. This data is the table including redshifts $z = z_i$ and distance moduli μ_i with errors σ_i for $N_S = 580$ supernovae. The distance modulus $\mu_i = \mu(D_L) = 5\log_{10}\big(D_L/10\mathrm{pc}\big)$ is logarithm of the luminosity distance [8, 27]:

$$D_L(z) = \frac{c\,(1+z)}{H_0} S_k\left(H_0 \int\limits_0^z \frac{d\tilde{z}}{H(\tilde{z})}\right). \tag{1}$$

Here

$$S_k(x) = \begin{cases} \sinh\big(x\sqrt{\Omega_k}\big)\big/\sqrt{\Omega_k}, & \Omega_k > 0, \\ x, & \Omega_k = 0, \\ \sin\big(x\sqrt{|\Omega_k|}\big)\big/\sqrt{|\Omega_k|}, & \Omega_k < 0; \end{cases}$$

redshift z and the Hubble parameter $H(z)$ are connected with the scale factor $a(t)$:

$$a(t) = \frac{a_0}{1+z}, \qquad H(z) = \frac{\dot{a}(t)}{a(t)}; \tag{2}$$

k is the sign of curvature, $\Omega_k = -k\big/(a_0^2 H_0^2)$ is its present time fraction, $a_0 \equiv a(t_0)$ and $H_0 \equiv H(t_0)$ are the current values of a and H.

We use the luminosity distance (1) and $H(z)$ to calculate the distance [6, 7, 8]

$$D_V(z) = \left[\frac{czD_L^2(z)}{(1+z)^2 H(z)}\right]^{1/3}, \tag{3}$$

and two measured values

$$d_z(z) = \frac{r_s(z_d)}{D_V(z)}, \qquad A(z) = \frac{H_0\sqrt{\Omega_m}}{cz} D_V(z), \tag{4}$$

which are usually considered as observational manifestations of baryon acoustic oscillations (BAO) [7, 6]. Here $\Omega_m = \frac{8}{3}\pi G\rho(t_0)/H_0^2$ is is the present time fraction of matter with density ρ. The value $r_s(z_d)$ in Eq. (4) is sound horizon size at the end of the drag era $z_d \simeq 1059.3$ [8]. Below we use

$$r_s(z_d) = 150.51 \pm 3.11 \text{ Mpc}, \tag{5}$$

that is the arithmetic average of the following recent estimations: $r_s(z_d) = 147.4$ [26], 147.49 [8, 25], 148.2 [14], 153.19 [23], 153.3 [11], 153.5 [10].

In this paper we consider 14 data points for $d_z(z)$ (7 recent points in addition to 7 ones in Ref. [32]) and 7 data points for $A(z)$ presented in the following table:

Table 1: Values of $d_z(z) = r_s(z_d)/D_V(z)$ and $A(z)$ (4) with errors [6]–[26]

z	$d_z(z)$	σ_d	$A(z)$	σ_A	Refs
0.106	0.336	0.015	0.526	0.028	[6] 6dFGS
0.15	0.2232	0.0084	-	-	[14] SDSS DR7
0.20	0.1905	0.0061	0.488	0.016	[6] SDSS LRG
0.275	0.1390	0.0037	-	-	[9] SDSS DR7
0.278	0.1394	0.0049	-	-	[10] SDSS DR7
0.314	0.1239	0.0033	-	-	[11] WiggleZ
0.32	0.1181	0.0023	-	-	[13] BOSS DR11
0.35	0.1097	0.0036	0.484	0.016	[9] SDSS DR7
0.35	0.1126	0.0022	-	-	[6] SDSS DR7
0.44	0.0916	0.0071	0.474	0.034	[11] WiggleZ
0.57	0.07315	0.0012	0.436	0.017	[6, 12] SDSS DR9
0.60	0.0726	0.0034	0.442	0.020	[11] WiggleZ
0.73	0.0592	0.0032	0.424	0.021	[11] WiggleZ
2.34	0.0320	0.00068	-	-	[26] BOSS DR11

For any cosmological model we fix its model parameters $p_1, p_2, \dots$, calculate dependence $a(t)$, the integral (1) and this model predicts theoretical values D_L^{th} for luminosity distance (1) (for given z), or μ^{th} for modulus, d_z^{th} and A^{th} for parameters (4). Then we are to compare these theoretical values with the observational data z_i and μ_i from the table [4] or with $d_z(z_i)$ and $A(z_i)$ from Table 1.

For this purpose and also for achievement a good fit between theoretical predictions and the observed data we use the χ^2 function, in particular, for the Type Ia supernovae data [4] in the form

$$\chi^2_S(p_1, p_2, \dots) = \sum_{i=1}^{N_S} \frac{\left[\mu_i - \mu^{th}(z_i, p_1, p_2, \dots)\right]^2}{\sigma_i^2}. \tag{6}$$

We search minimum of χ^2 in the space of model parameters $p_1, p_2, \dots$ or the maximum of the corresponding likelihood function $\mathcal{L}_S(p_1, p_2, \dots) = \exp(-\chi^2_S/2)$.

Measurements of $d_z(z)$ and $A(z)$ from Ref. [11] in Table 1 are not independent (unlike the mentioned supernovae data). So the χ^2 function for the values (4) is

$$\chi^2_B(p_1, p_2, \dots) = (\Delta d)^T C_d^{-1} \Delta d + (\Delta A)^T C_A^{-1} \Delta A, \qquad \Delta d = d_z(z_i) - d_z^{th}. \tag{7}$$

The elements of covariance matrices $C_d^{-1} = ||c^d_{ij}||$ and $C_A^{-1} = ||c^A_{ij}||$ with $i, j = 10, 12, 13$ in Eq. (7) are [6, 11]:

$$\begin{array}{llll} c^d_{1010} = 24532.1, & c^d_{1012} = -25137.7, & c^d_{1013} = 12099.1, & c^d_{1212} = 134598.4, \\ c^d_{1213} = -64783.9, & c^d_{1313} = 128837.6; & c^A_{1010} = 1040.3, & c^A_{1012} = -807.5, \\ c^A_{1013} = 336.8, & c^A_{1212} = 3720.3, & c^A_{1213} = -1551.9, & c^A_{1313} = 2914.9. \end{array}$$

Here $c_{ij} = c_{ji}$, the remaining matrix elements are $c_{ii} = 1/\sigma_i^2$, $c_{ij} = 0$, $i \neq j$.

Measurements of the Hubble parameter $H(z)$ for different redshifts z [15]–[26] with 34 data points are presented in the following table:

Table 2: Values of the Hubble parameter $H(z)$ with errors σ_H from Refs. [15]–[26]

z	$H(z)$	σ_H	Refs	z	$H(z)$	σ_H	Refs
0.070	69	19.6	[19]	0.57	92.9	7.855	[23]
0.090	69	12	[15]	0.593	104	13	[17]
0.120	68.6	26.2	[19]	0.600	87.9	6.1	[18]
0.170	83	8	[15]	0.680	92	8;	[17]
0.179	75	4	[17]	0.730	97.3	7.0	[18]
0.199	75	5	[17]	0.781	105	12	[17]
0.200	72.9	29.6	[19]	0.875	125	17	[17]
0.240	79.69	2.65	[22]	0.880	90	40	[16]
0.270	77	14	[15]	0.900	117	23	[15]
0.280	88.8	36.6	[19]	1.037	154	20	[17]
0.300	81.7	6.22	[24]	1.300	168	17	[15]
0.350	82.7	8.4	[21]	1.430	177	18	[15]
0.352	83	14	[17]	1.530	140	14	[15]
0.400	95	17	[15]	1.750	202	40	[15]
0.430	86.45	3.68	[22]	2.300	224	8	[20]
0.440	82.6	7.8	[18]	2.340	222	7	[26]
0.480	97	62	[16]	2.360	226	8	[25]

These values $H(z)$ were calculated with evaluation of the age difference for galaxies with close redshifts via the formula $H(z) = \dfrac{1}{a(t)}\dfrac{da}{dt} = -\dfrac{1}{1+z}\dfrac{dz}{dt}$ (resulting from Eq. (2)) in Refs. [15]–[21] or from BAO analysis [22]–[26].

3. ΛCDM model

For the ΛCDM model the Einstein equations

$$G^\mu_\nu = 8\pi G T^\mu_\nu + \Lambda\delta^\mu_\nu, \tag{8}$$

determine dynamics of the Universe. Here $G^\mu_\nu = R^\mu_\nu - \frac{1}{2}R\delta^\mu_\nu$ is the Einstein tensor,

$$T^\mu_\nu = \mathrm{diag}\,(-\rho, p, p, p) \tag{9}$$

is the energy momentum tensor. In this model baryonic and dark matter may be considered as one component of dust-like matter with density $\rho = \rho_b + \rho_{dm}$, so we suppose $p = 0$ in Eq. (9). The fraction of relativistic matter (radiation and neutrinos) is close to zero for observable values $z \le 2.36$.

For the Robertson-Walker metric with the curvature sign k

$$ds^2 = -dt^2 + a^2(t)\Big[(1 - kr^2)^{-1}dr^2 + r^2 d\Omega\Big] \tag{10}$$

the Einstein equations (8) are reduced to the system

$$3\frac{\dot a^2 + k}{a^2} = 8\pi G\rho + \Lambda, \tag{11}$$

$$\dot\rho = -3\frac{\dot a}{a}(\rho + p). \tag{12}$$

Eq. (12) results from the continuity condition $T^\mu_{\nu;\mu} = 0$, the dot denotes the time derivative, here and below the speed of light $c = 1$.

For dust-like matter with pressure $p = 0$ we use the solution $\rho/\rho_0 = (a/a_0)^{-3}$ of Eq. (12) and rewrite the remaining equation Eq. (11) in the form

$$\frac{\dot a^2}{a^2 H_0^2} = \frac{H^2}{H_0^2} = \Omega_m\Big(\frac{a}{a_0}\Big)^{-3} + \Omega_\Lambda + \Omega_k\Big(\frac{a}{a_0}\Big)^{-2}. \tag{13}$$

Here the present time fractions of matter, dark energy (Λ term) and curvature

$$\Omega_m = \frac{8\pi G\rho(t_0)}{3H_0^2}, \qquad \Omega_\Lambda = \frac{\Lambda}{3H_0^2}, \qquad \Omega_k = -\frac{k}{a_0^2 H_0^2} \tag{14}$$

are connected by the equality

$$\Omega_m + \Omega_\Lambda + \Omega_k = 1, \tag{15}$$

resulting from Eq. (13) if we fix $t = t_0$.

We solve the equation (13) with the natural initial condition at the present time $a(t_0) = a_0$ and three fixed model parameters H_0, Ω_m and Ω_Λ. As the result we calculate the values $a(t)/a_0$, $H(t)$, $H(z)$, and also $D_L(z)$ (1), $d_z(z)$ and $A(z)$ (4).

Further we compare them with the observational data from Ref. [4] and Tables 1, 2 with the help of the χ^2 functions (6), (7) and their analog

$$\chi^2_H(p_1, p_2, \dots) = \sum_{i=1}^{N_H} \frac{\big[H_i - H^{th}(z_i, p_1, p_2, \dots)\big]^2}{\sigma^2_{H,i}}. \tag{16}$$

Here $N_H = 34$ for all data points in Table 2.

If we introduce dimensionless time τ and logarithm of the scale factor [30, 31]

$$\tau = H_0 t, \qquad \mathcal{A} = \log\frac{a}{a_0}. \tag{17}$$

equation (13) will take the form

$$\frac{d\mathcal{A}}{d\tau} = \sqrt{\Omega_m e^{-3\mathcal{A}} + \Omega_\Lambda + \Omega_k e^{-2\mathcal{A}}},$$

more convenient for numerical solving with the initial condition $\mathcal{A}\big|_{\tau=1} = 0$. Here and below the present time $t = t_0$ corresponds to $\tau = 1$.

To describe the considered observational data we use the mentioned three independent parameters H_0, Ω_m and Ω_Λ in Eq. (13) of the ΛCDM model. The curvature fraction Ω_k is expressed from Eq. (15). The Hubble constant H_0 is the very important parameter in all cosmological models, but different approaches result in wide spread of its estimations. In particular, the satellite projects Planck Collaboration (Planck) [8], Wilkinson Microwave Anisotropy Probe (WMAP) [6] and Hubble Space Telescope (HST) [33] give the following values (in km c^{-1}Mpc^{-1}):

$$H_0 = 67.3 \pm 1.2 \text{ (Planck) [8]}, \quad 69.7 \pm 2.4 \text{ (WMAP) [6]}, \quad 73.8 \pm 2.4 \text{ (HST) [33]}. \tag{18}$$

The best fits for parameters H_0, Ω_m and Ω_Λ of the ΛCDM model was calculated in many papers, in particular, in Refs. [6, 8, 34, 35, 36, 37] for describing the Type Ia supernovae, $H(z)$ and BAO data in various combinations. The authors [36, 37] compared the ΛCDM model with the XCDM and ϕCDM models. They fixed two values of the Hubble constant $H_0 = 68 \pm 2.8$ and $H_0 = 73.8 \pm 2.4$ km c^{-1}Mpc^{-1} [33] and searched optimal choice of other model parameters. But they did not estimated the segment between these two values of H_0. The authors [35] compared 8 models with two information criteria including minimal χ^2 and the number of model parameters. They calculated optimal values of these parameters with the exception of H_0, though H_0 is the important parameter for all 8 models.

In this paper we study in detail the dependence of the χ^2 minimal value on H_0. This dependence is very important if we compare different cosmological models.

We present the results of calculations as level lines for the function $\chi^2(p_1, p_2)$ in a plane of two parameters, for example, $\chi^2(\Omega_m, \Omega_\Lambda)$, if H_0 is fixed (see Fig. 1). In accordance with usual approach [6, 8, 34, 35, 36, 37] we draw level lines for $\chi^2(p_1, p_2)$ or $\mathcal{L}(p_1, p_2) = \exp(-\chi^2/2)$ o at 1σ (68.27%), 2σ (95.45%) and 3σ (99.73%) confidence levels.

In Fig. 1 we use this scheme for 3 fixed values H_0 indicated on the panels (2 values (18) and the optimal value $H_0 = 70.20$ km c^{-1}Mpc^{-1}). If H_0 is fixed, we draw level lines of functions (6), (7), (16) (the top panels in Fig. 1) and their sum

$$\chi^2_\Sigma = \chi^2_S + \chi^2_H + \chi^2_B \qquad (19)$$

(the second row of panels) as functions of two remaining parameters Ω_m and Ω_Λ.

In the right third panel we fix the optimal value $\Omega_\Lambda = 0.769$ and draw level lines for $\chi^2_\Sigma(\Omega_m, H_0)$, in the right bottom panel for fixed $\Omega_m = 0.276$ we present level lines for $\chi^2_\Sigma(\Omega_\Lambda, H_0)$.

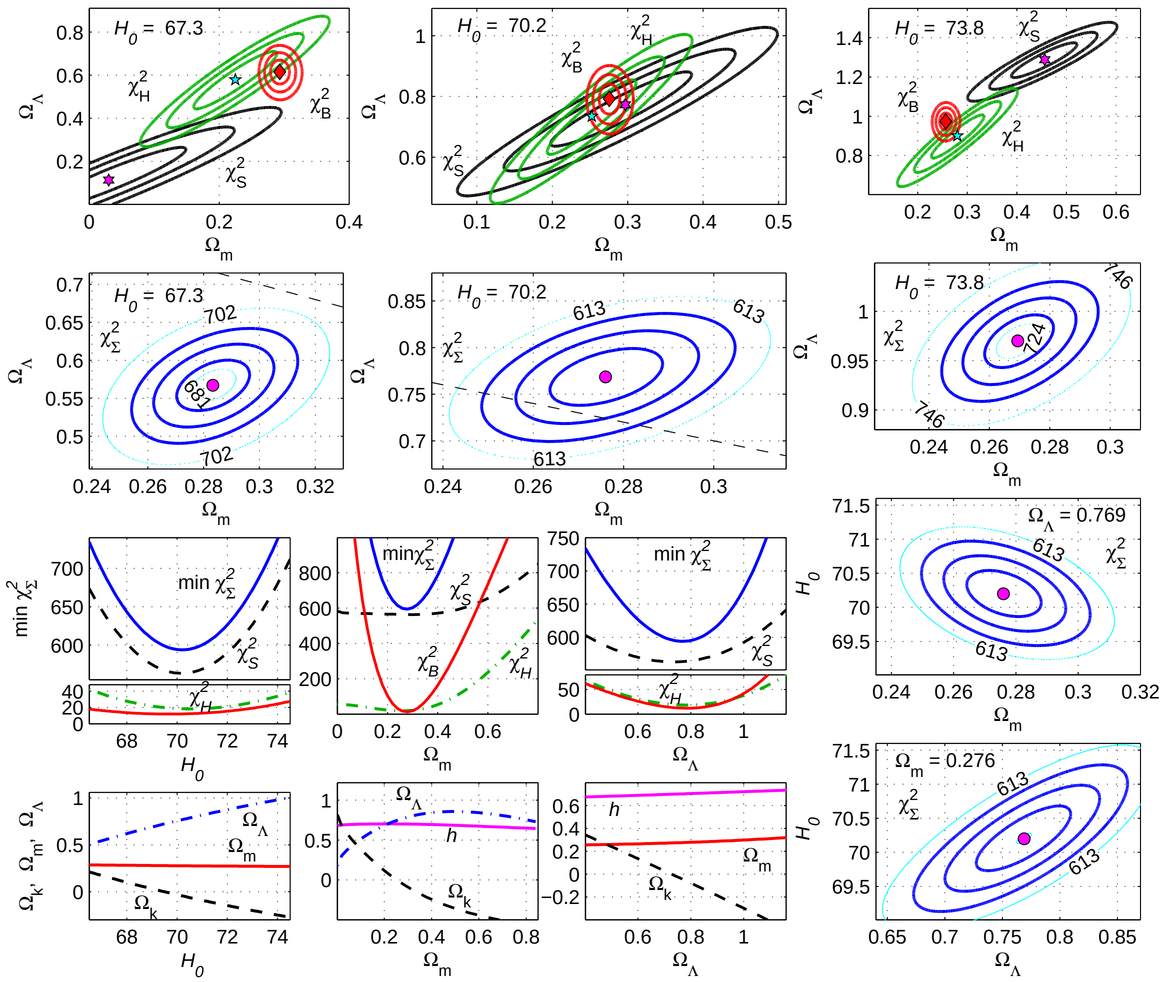

Figure 1: The ΛCDM model. For 3 indicated values H_0 level lines are drawn at 1σ, 2σ and 3σ (thick solid) for $\chi^2_S(\Omega_m, \Omega_\Lambda)$ (black), for $\chi^2_H(\Omega_m, \Omega_\Lambda)$ (green) and $\chi^2_B(\Omega_m, \Omega_\Lambda)$ (red in the top line), the sum (19) $\chi^2_\Sigma(\Omega_m, \Omega_\Lambda)$ (the second row), $\chi^2_\Sigma(\Omega_m, H_0)$ for $\Omega_\Lambda = 0.758$ and $\chi^2_\Sigma(\Omega_\Lambda, H_0)$ for $\Omega_m = 0.276$ (the bottom-right panels); dependence of $\min \chi^2_\Sigma$ (blue thick lines), its fractions χ^2 and parameters of a minimum point on H_0, Ω_m and on Ω_Λ.

In these panels of Fig. 1 the points of minima are marked in as hexagrams for

χ^2_S, pentagrams for χ^2_H, diamonds for χ^2_B and circles for χ^2_Σ.

Minimal values of the function χ^2_Σ (19) for 3 values H_0 (18) and for the optimal value $H_0 = 70.2$ are tabulated in Table 3 so we can compare efficiency of this description for different H_0. For the same purpose we point out the corresponding values for some level lines of χ^2_Σ and present the dependence of the minimum $\min\chi^2_\Sigma = \min\limits_{\Omega_m,\Omega_\Lambda}\chi^2_\Sigma(H_0)$ on H_0 in the left third panel of Fig. 1. We also show in this panel graphs of the fractions χ^2_S (the black dashed line), χ^2_H (the green dash-and-dot line), χ^2_B (the red line) in the value $\min\chi^2_\Sigma(H_0)$.

We see in Fig. 1 and in Table 3 that the dependence of $\min\chi^2_\Sigma(H_0)$ is significant. This function has the distinct minimum and achieves its minimal value 593.91 at $H_0 \simeq 70.2$ km c^{-1}Mpc^{-1} and the following optimal parameters:

$$\Lambda\text{CDM}: \quad H_0 = 70.20, \quad \Omega_m = 0.276, \quad \Omega_\Lambda = 0.769, \quad \Omega_k = -0.045. \qquad (20)$$

This point of minimum lies between the values $H_0 = 68$ and $H_0 = 73.8$ km c^{-1}Mpc^{-1} chosen in Refs. [36, 37], so that choice was unsuccessful.

The sharp dependence of $\min\chi^2_\Sigma$ on H_0 is connected with two factors: (1) the similar dependence of the main contribution $\chi^2_S(H_0)$ shown in the same panel as the black dashed line; (2) the large shift of the minimum point for χ^2_S in the Ω_m, Ω_Λ plane corresponding to H_0 growth (see the top line in Fig. 1). For $H_0 = 67.3$ and 73.8 km c^{-1}Mpc^{-1} this minimum point is far from the similar points of χ^2_H and χ^2_B. Only for H_0 close to 70 km c^{-1}Mpc^{-1} all these three minimum points (hexagrams, pentagrams and diamonds in Fig. 1) are close to each other.

In other two panels in the third line of Fig. 1 we present how minima $\min\chi^2_\Sigma$ depend on Ω_m and on Ω_Λ. Here $\min\chi^2_\Sigma(\Omega_m) = \min\limits_{H_0,\Omega_\Lambda}\chi^2_\Sigma$, $\min\chi^2_\Sigma(\Omega_\Lambda) = \min\limits_{\Omega_m,H_0}\chi^2_\Sigma$; graphs of the fractions χ^2_S, χ^2_H, χ^2_B in $\min\chi^2_\Sigma$ are also shown.

In the bottom panels of Fig. 1 we demonstrate how parameters of a minimum point of χ^2_Σ depend on H_0, Ω_m and on Ω_Λ. The parameter Ω_k is determined from Eq. (15): $\Omega_k = 1 - \Omega_m - \Omega_\Lambda$. When we vary parameters Ω_m and Ω_Λ, we also draw the graphs $h(\Omega_m)$ and $h(\Omega_\Lambda)$, where $h = H_0/100$ and H_0 is the optimal value corresponding to the minimum point of χ^2_Σ.

Fig. 1 demonstrates that dependencies of $\min\chi^2_\Sigma$ on Ω_m and Ω_Λ have the same sharp minimum as for $\min\chi^2_\Sigma(H_0)$. The most distinct minimum we see for dependence $\min\limits_{H_0,\Omega_\Lambda}\chi^2_\Sigma$ on Ω_m because of the correspondent dependence of its fraction χ^2_B (the red line). This fact for χ^2_B is connected with the contribution from the value $A(z)$ (4) measurements, because $A(z)$ is proportional to $\sqrt{\Omega_m}$ and χ^2_B is very sensitive to Ω_m values. Note that the fractions χ^2_S and χ^2_H (in $\min\chi^2_\Sigma$) weakly depend on Ω_m.

In the 2-nd row panels of Fig. 1 with χ^2_Σ the flatness line $\Omega_m + \Omega_\Lambda = 1$ (or $\Omega_k = 0$) is shown as the black dashed straight line. This line demonstrates that only for H_0 close to 70 km c^{-1}Mpc^{-1} the ΛCDM model satisfies on 1σ or 2σ level the following recent observational limitations on the parameters (14) [6, 8]:

$$\text{WMAP [6]:}\quad \begin{array}{l}\Omega_m = 0.279 \pm 0.025,\\ \Omega_\Lambda = 0.721 \pm 0.025,\\ \Omega_k = -0.0027^{+0.0039}_{-0.0038};\end{array} \qquad \text{Planck [8]:}\quad \begin{array}{l}\Omega_m = 0.314 \pm 0.02\\ \Omega_\Lambda = 0.686 \pm 0.025,\\ \Omega_k = -0.0005^{+0.0065}_{-0.0066}.\end{array} \qquad (21)$$

For $H_0 = 67.3$ and 73.8 km c^{-1}Mpc^{-1} the optimal values of parameters Ω_m, Ω_Λ, Ω_k in Table 3 are far from restrictions (21) even on 3σ level.

At the right hand side of Table 3 we tabulate the same estimations of $\min \chi^2_\Sigma$ Minimal and optimal values Ω_i for the reduced data set satisfying the condition $z < 2.3$. For these calculations we exclude the data points from Refs. [20, 25, 26] from Tables 1 and 2.

Table 3: The ΛCDM model. For all data points in Tables 1, 2 (left) and for 31 data points of $H(z)$ and 13 of $d_z(z)$ with $z < 2.3$ (right) for 3 given H_0 (18) and the optimal value $H_0 = 70.2$ km c^{-1}Mpc^{-1} we demonstrate the calculated minima of χ^2_Σ with Ω_m, Ω_Λ, Ω_k correspondent to $\min \chi^2_\Sigma$.

	$N_H = 34$				$N_H = 31 \quad (z < 2.3)$			
H_0	$\min \chi^2_\Sigma$	Ω_m	Ω_Λ	Ω_k	$\min \chi^2_\Sigma$	Ω_m	Ω_Λ	Ω_k
67.3	680.08	0.283	0.567	0.150	658.86	0.301	0.533	0.166
69.7	596.55	0.277	0.737	−0.014	593.35	0.284	0.726	−0.010
70.2	593.91	0.276	0.769	−0.045	592.42	0.281	0.762	−0.043
73.8	723.04	0.269	0.970	−0.307	713.23	0.260	0.986	−0.246

4. Multidimensional model

I. Pahwa, D. Choudhury and T.R. Seshadri in Ref. [30] suggested the multidimensional gravitational model (the PCS model in references below) with symmetry and isotropy in 3 usual spatial dimensions and in d additional dimensions. But there is anisotropy between these subspaces: matter behaves like dust in usual dimensions and has negative pressure p_e in extra dimensions in the form [32]

$$T^\mu_\nu = \mathrm{diag}\,(-\rho, 0, 0, 0, p_e, \dots, p_e), \qquad \rho = \rho_b + \rho_e, \qquad p_e = -B_0 {\rho_e}^{-\alpha}. \qquad (22)$$

In this paper we divide matter in two components following Ref. [32]: the "usual" or "baryonic" component with density ρ_b and $p_b = 0$ (it may include a part of cold dark matter) and the "exotic" component with ρ_e and pressure p_e in extra dimensions. The "exotic" matter plays roles of both dark matter and dark energy.

For the spacetime with $1 + 3 + d$ dimensions the metric [30]

$$ds^2 = -dt^2 + a^2(t)\left(\frac{dr^2}{1 - kr^2} + r^2 d\Omega\right) + b^2(t)\left(\frac{dR^2}{1 - k_2 R^2} + R^2 d\Omega_{d-1}\right) \qquad (23)$$

includes two Robertson–Walker terms with two scale factors $a(t)$, $b(t)$ and two curvature signs k, k_2 for usual in extra dimensions correspondingly.

The main advantage of this model is the natural dynamical compactification for cosmological solutions [31], in other words, the scale factor $a(t)$ grows while $b(t)$ rapidly diminishes. We suppose that the value $b(t)$ is small enough at present time.

Dynamics of the models [30, 31] results from the Einstein equations (9) with $\Lambda = 0$ and the energy momentum tensor (22). If we use the dimensionless notations (17) and

$$\mathcal{B} = \log\frac{b}{b_0}, \qquad \bar\rho_b = \frac{\rho_b}{\rho_{cr}}, \qquad \bar\rho_e = \frac{\rho_e}{\rho_{cr}}, \qquad \bar p_e = \frac{p_e}{\rho_{cr}}, \qquad \rho_{cr} = \frac{3H_0^2}{8\pi G} \tag{24}$$

(where $b_0 = b(t_0)$) equations (9) for $k_2 = 0$ and $d > 1$ will take the form [32]:

$$\begin{aligned}
\mathcal{A}'' &= \tfrac{1}{d+2}\Big[d(d-1)\,\mathcal{B}'\big(\tfrac12\mathcal{B}' - \mathcal{A}'\big) - 3(d+1)\,\mathcal{A}'^2 - 3d\bar p_e + (2d+1)\Omega_k e^{-2\mathcal{A}}\Big], && (25)\\
\bar\rho_b' &= -\bar\rho_b(3\mathcal{A}' + d\mathcal{B}'), \qquad \bar\rho_e' = -3\bar\rho_e\mathcal{A}' - d(\bar\rho_e + \bar p_e)\,\mathcal{B}', && (26)\\
\mathcal{B}' &= (d-1)^{-1}\Big[-3\mathcal{A}' + \sqrt{3\big[(d+2)\,\mathcal{A}'^2 + 2(d-1)\,(\bar\rho + \Omega_k e^{-2\mathcal{A}})\big]/d}\Big]. && (27)
\end{aligned}$$

In the important case $d = 1$ (omitted in Ref. [30]) we use the equation [31]

$$\mathcal{B}' = (\bar\rho + \Omega_k e^{-2\mathcal{A}})/\mathcal{A}' - \mathcal{A}' \tag{28}$$

instead of Eq. (27). The power law dependence (22) takes the form $\bar p_e = -B/\bar\rho_e{}^\alpha$.

Initial conditions for the system (25) – (27) at the present time $\tau = 1$ (corresponding to $t = t_0$) are

$$\bar\rho\big|_{\tau=1} = \Omega_m, \qquad \bar\rho_b\big|_{\tau=1} = \Omega_b, \qquad \mathcal{A}\big|_{\tau=1} = 0, \qquad \mathcal{A}'\big|_{\tau=1} = 1. \tag{29}$$

They result from definitions (14), (17), (24) and $\mathcal{A}'(\tau) = \dfrac{d}{d\tau}\log\dfrac{a}{a_0} = \dfrac{1}{H_0}\dfrac{\dot a}{a}$.

For the model PCS [30, 31] we have the analog of Eq. (15)

$$\Omega_m + \Omega_B + \Omega_k = 1, \tag{30}$$

resulting from Eqs. (27) or (28) at $\tau = 1$. Here $\Omega_B = -d\big(\mathcal{B}' + \frac{d-1}{6}\mathcal{B}'^2\big)\big|_{\tau=1}$ is the contribution from d extra dimensions.

If we solve numerically the system (25) – (28) with given initial conditions (29), we obtain functions $a(\tau)$, $b(\tau)$, $\rho(\tau)$, describing this cosmological solution. These solutions with optimal parameters from Table 4 for the PCS model with $d = 1$ and $d = 2$ (in comparison with the ΛCDM model) are shown in Fig. 2.

Cosmological solutions in the PCS model are divided into two classes [31]: regular solutions describe the standard Big Bang with the scale factor a starting from $a = 0$ (this point corresponds to infinite values of b and ρ), singular solutions start from nonzero a, corresponding to $\rho \to \infty$ and $b = 0$. So singular solutions are not physical.

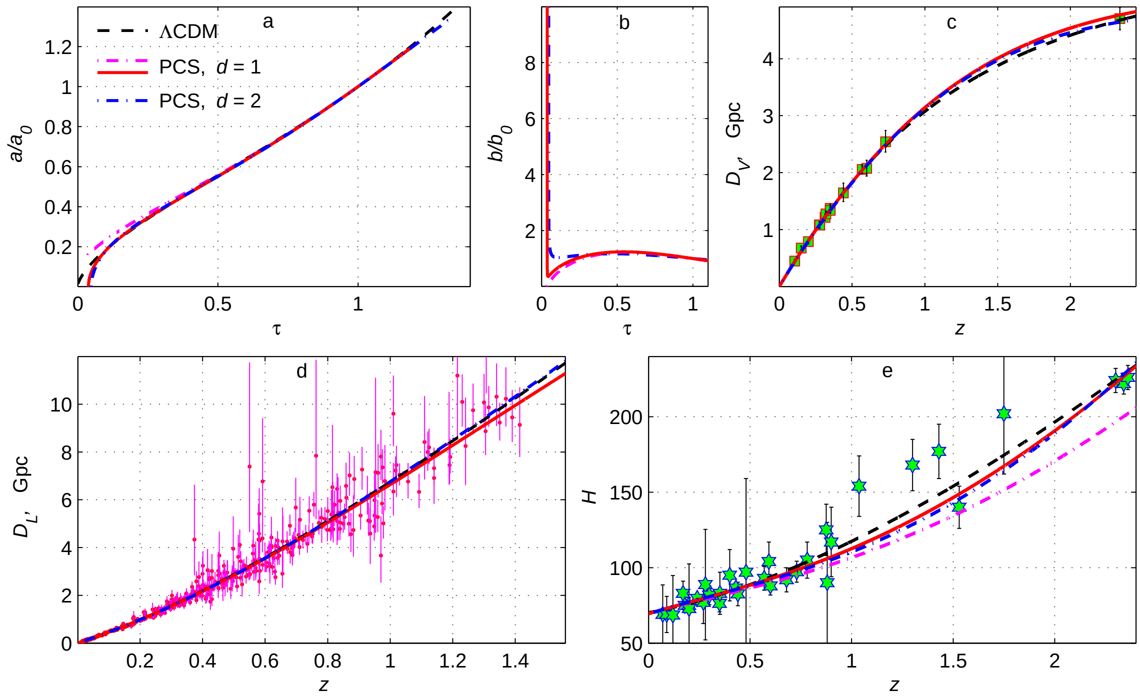

Figure 2: Cosmological solutions for the models ΛCDM (black dashed lines), PCS with $d = 1$ (red lines) and $d = 2$ (blue dash-and-dot lines) with the optimal values of model parameters (20) and from Table 4: the scale factors (a) $a(\tau)$, (b) $b(\tau)$; (c) the distance (3) $D_V(z)$ with the data points from Table 1 (d) the luminosity distance $D_L(z)$ and the Type Ia supernovae data [4]; (e) dependence $H(z)$ with the data points from Table 2.

In Fig. 2 red and blue lines describe regular solutions with $d = 1$ and $d = 2$ and parameters from Table 4; whereas the violet dashed lines describe the singular solution with $d = 1$ and the following parameters: $H_0 = 69.45$, $\Omega_m = 0.286$, $\Omega_b = 0.047$, $\Omega_k = -0.08$, $\alpha = -0.26$, $B = 2.17$. Here only the value B differs from the optimal value in Table 4 (the regular solution with these optimal parameters is shown as the solid red lines), other values are the same.

On can see in Fig. 2 that predictions of the PCS model with $d = 1$ (solid red lines) and with $d = 2$ (blue dash-and-dot lines) with parameters from Table 4 (all data) are very close to the black dashed curves, corresponding to the ΛCDM model with parameters (20).

The PCS model has the set of model parameters H_0, Ω_b, Ω_m, Ω_k, α, B, but also it has the additional integer-valued parameter d (the number of extra dimensions). Our calculations of optimal parameters in Table 4 demonstrate that the value $d = 1$ is the most preferable for describing the observational data for supernovae, BAO and $H(z)$. So it is the case $d = 1$ that we present in detail in Fig. 3.

The parameter Ω_b in this model may include not only the visible baryon fraction, but also a part of dark matter. In 3 bottom-right panels of Fig. 3 we investigate influence of Ω_b on the model behavior, in particular, the dependence of minimum

$\min\chi^2_\Sigma$ (over all other parameters) on Ω_b. The blue solid curve corresponds to all data from Tables 1, 2, the red dash-and-dot line describes only data with $z \le 2.3$. As one can see, $\min\chi^2_\Sigma$ increases when Ω_b grows, but this dependence is rather weak for small Ω_b. So for the multidimensional model PCS we fix $\Omega_b = 0.047$ that is the simple average of the WMAP $\Omega_b = 0.0464$ [6] and Planck $\Omega_b = 0.0485$ [8] estimations. The value $\Omega_b = 0.047$ is fixed in all panels of Fig. 3 (except for the mentioned 3 bottom-right panel) and really we use only 5 remaining parameters H_0, Ω_m, Ω_k, α, B.

For level lines of χ^2_Σ and other χ^2 in the top and right panels of Fig. 3 we use the same notations as in Fig. 1. We draw these lines for $H_0 = 67.3$, 73.8 (18) and the optimal value $H_0 = 69.45$ km c^{-1}Mpc^{-1} in the α, B plane and also level lines of χ^2_Σ for the optimal values of parameters (see Table 4) in α, H_0; Ω_k, H_0 and Ω_b, H_0 planes.

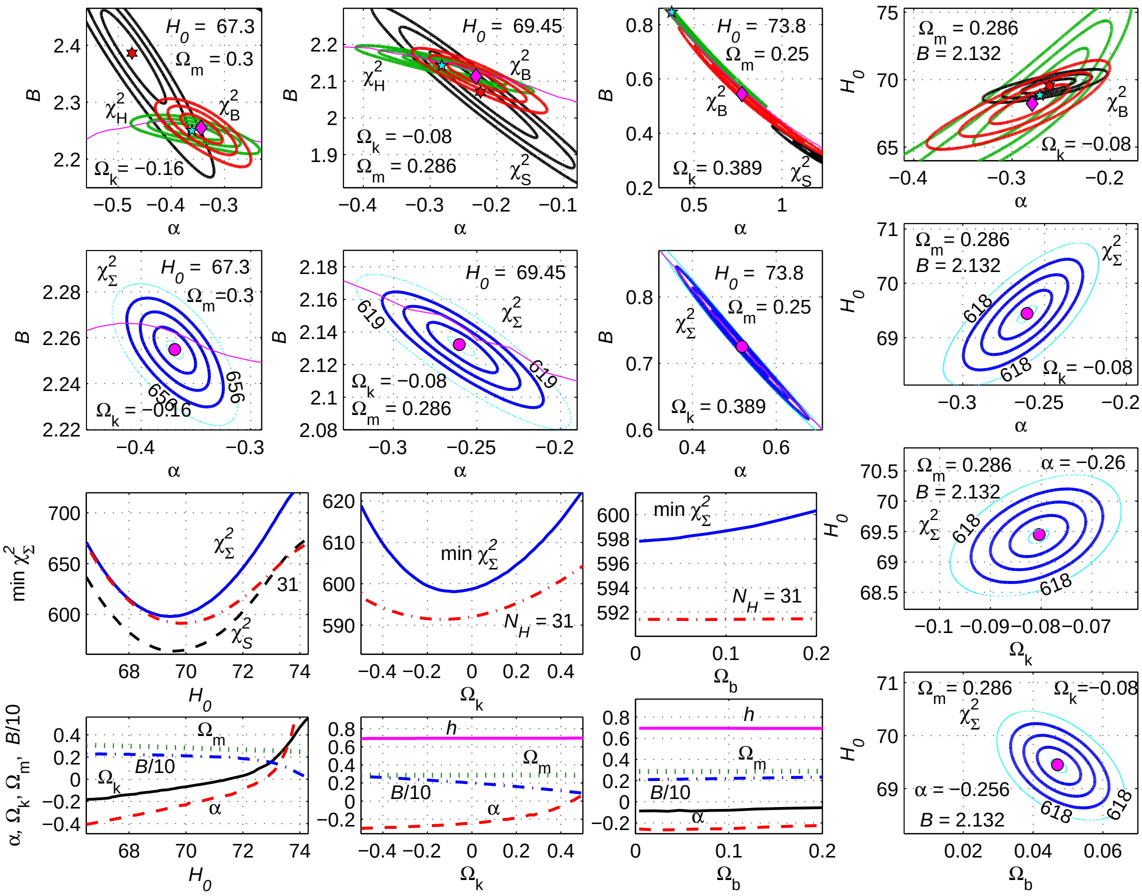

Figure 3: The PCS model with $d = 1$. For H_0 (18) and the optimal value $H_0 = 69.45$ km c^{-1}Mpc^{-1} level lines of χ^2_Σ and other χ^2 are presented in α, B; α, H_0; Ω_k, H_0 and Ω_b, H_0 planes in notations of Fig. 1. In the bottom-left panels we analyze dependence of $\min\chi^2_\Sigma$ and parameters of a minimum point on H_0, Ω_k and Ω_b.

In 6 top-left panels of Fig. 3 we draw thin purple lines dividing domain of regular solutions on the α, B plane (below these lines) and the upper domain (for larger B) of singular solutions. The singular solutions have singularities in the past with $\rho \to \infty$ corresponding to $a \neq 0$ [31], so they are nonphysical and should be excluded. Note that the optimal solutions in Table 4 lie near this border, but they are regular and describe the standard Big Bang $\rho \to \infty \;\Leftrightarrow\; a \to 0$ with dynamical compactification of extra dimensions.

The dependence of $\min\chi^2_\Sigma = \min\limits_{\Omega_m,\Omega_k,\alpha,B}\chi^2_\Sigma$ on H_0 for $d = 1$ has the distinct minimum at $H_0 \simeq 69.45$ (the solid blue line in the panel) similarly to the case of the ΛCDM model in Fig. 1. The minimal value $\min\chi^2_\Sigma \simeq 598.08$ for $d = 1$ is larger than $\min\chi^2_\Sigma = 593.91$ (20) for the ΛCDM model; and for $d \geq 2$ the minima are still worse (see Table 4).

One may conclude that the results for the PCS model are worse than for the ΛCDM, but this conclusion depends on a data selection. In particular, any comparison of these models is very sensitive to BAO and $H(z)$ data with high z ($z > 2$). If we exclude 3 data points [20, 25, 26] for $H(z)$ with $z > 2$ and the corresponding point $d_z(z = 2.34) = 0.032$ [26] from Table 1, we obtain other values presented at the right side of Table 3 and in Table 4. We see that under the data restriction $z < 2.3$ the PCS model yields better fit than the ΛCDM.

In Fig. 3 all presented level lines and graphs correspond to all data with $N_H = 34$ with only exceptions for dependencies of $\min\chi^2_\Sigma$ on H_0, Ω_k and Ω_b, where graphs for all data with $N_H = 34$ are solid blue lines, but the similar graphs for restricted data with $N_H = 31$ are shown as red dash-and-dot lines. The minimum values for these lines are in Table 4.

Table 4: Optimal values of model parameters for the PCS model [30], $\Omega_b = 0.047$.

	$N_H = 34$ (all data)					
d	$\min\chi^2_\Sigma$	H_0	Ω_m	Ω_k	α	B
1	598.08	69.45	0.286	−0.080	−0.260	2.132
2	601.04	69.27	0.288	−0.154	−0.392	1.746
3	602.52	69.22	0.289	−0.101	−0.438	1.525
6	603.85	69.17	0.289	−0.118	−0.498	1.366
	$N_H = 31$ ($z < 2.3$)					
d	$\min\chi^2_\Sigma$	H_0	Ω_m	Ω_k	α	B
1	591.41	69.86	0.281	−0.141	−0.177	2.123
2	591.76	69.77	0.282	−0.135	−0.289	1.630
3	591.95	69.75	0.282	−0.138	−0.337	1.467
6	592.15	69.72	0.282	−0.146	−0.393	1.286

5. Conclusion

In this paper we used the ΛCDM and the multidimensional PCS model [30] for describing the observational data for type Ia supernovae [4], BAO (Table 1) and $H(z)$ (Table 2). Here we included 14 BAO data points in Table 1 (in comparison with 7 data points in our previous investigation [32]).

When we calculated how absolute minimum (over other parameters) $\min\chi^2_\Sigma(p)$ depend on a fixed parameter p (see Figs. 1, 3), we obtained the following 1σ estimates for parameters of the ΛCDM and PCS ($d = 1$) models:

Table 5: 1σ estimates of model parameters ($\Omega_b = 0.047$ in the PCS model).

Model	$\min\chi^2_\Sigma$	H_0	Ω_k	Ω_m	other
ΛCDM	593.91	$70.20^{+0.319}_{-0.316}$	-0.045 ± 0.032	0.276 ± 0.008	$\Omega_\Lambda = 0.769^{+0.029}_{-0.03}$
PCS $_{d=1}$	598.08	$69.45^{+0.35}_{-0.34}$	-0.08 ± 0.045	0.286 ± 0.010	$\alpha = -0.26^{+0.03}_{-0.032}$

Our estimates for the ΛCDM are in agreement with the WMAP observational restrictions (21) on Ω_m, Ω_Λ, Ω_k [6], but they are in tension with the Planck data [8] (because of too low value $H_0 = 67.3$ km c^{-1}Mpc^{-1} in the Planck survey [8]).

On the expanded data base we confirmed the main conclusion of Ref. [32]: the ΛCDM model is the most effective in describing the mentioned observational data for type Ia supernovae, BAO and $H(z)$ if this data includes the estimations [20, 25, 26] of $H(z)$ and $d_z(z)$ for $z \ge 2.3$. In this case the minimal value $\min\chi^2_\Sigma = 593.91$ (20) for the ΛCDM is less than $\min\chi^2_\Sigma \simeq 598.08$ for the PCS model.

The weighty argument in favor of the ΛCDM is its small number N_p of model parameters (degrees of freedom). This number plays the important role in information criteria of model selection statistics, in particular, in the Akaike information criterion [35]:

$$AIC = \min\chi^2_\Sigma + 2N_p.$$

This criterion supports the leading position of the ΛCDM model.

On another hand, if we exclude the mentioned 4 data points with $z \ge 2.3$ [20, 25, 26] we shall obtain the minimum $\min\chi^2_\Sigma = 591.41$ for the PCS model less than the value 592.42 for the ΛCDM and the model PCS [30] describes the reduced set of data with $z < 2$ better than the ΛCDM. The best fit is for $d = 1$, the optimal value of $H_0 \simeq 69.86$ km c^{-1}Mpc^{-1}.

So the final conclusion about the effectiveness of the PCS model [30] depends on data selection and on possible model dependence of observational data, in particular, data for $z \ge 2.3$ from Refs. [20, 25, 26].

References

[1] Riess A.G. et al. *Observational Evidence from Supernovae for an Accelerating Universe and a Cosmological Constant.* Astron. J. 1998, **116**, 1009 (arXiv: astro-ph/9805201)

[2] Perlmutter S. et al. *Measurements of Omega and Lambda from 42 high redshift supernovae.* Astrophys. J. 1999, **517**, pp. 565 – 586 (arXiv: astro-ph/9812133)

[3] Kirshner R.P. *Foundations of supernova cosmology.* In Dark Energy – Observational and Theoretical Approaches. Ed. Pilar Ruiz-Lapuente. 2010, p.151, New York by Cambridge University Press (arXiv: 0910.0257)

[4] Suzuki N. et al. *The Hubble Space Telescope Cluster Supernova Survey: V. Improving the Dark Energy Constraints Above $z > 1$ and Building an Early-Type-Hosted Supernova Sample.* Astrophys. J. 2012, **746**, 85, 24pp. (arXiv: 1105.3470); http://supernova.lbl.gov/Union/

[5] Weinberg D.H. et al. *Observational Probes of Cosmic Acceleration.* Physics Reports 2013, **530**, pp. 87 – 255 (arXiv: 1201.2434)

[6] Hinshaw G. et al. *Nine-year Wilkinson Microwave Anisotropy Probe (WMAP) Observations: Cosmological Parameters Results.* Astrophysical Journal Suppl. 2013, **208**, 19, 25pp. (arXiv: 1212.5226)

[7] Eisenstein D.J. et al. *Detection of the baryon acoustic peak in the large-scale correlation function of SDSS luminous red galaxies.* Astrophys. J. 2005, **633**, pp. 560 – 574 (astro-ph/0501171)

[8] Ade P.A.R. et al. *Planck 2013 results. XVI. Cosmological parameters.* Astron. Astrophys. 2014, **571**, A16, 66pp. (arXiv: 1303.5076)

[9] Percival W.J. et al.*Baryon acoustic oscillations in the Sloan Digital Sky Survey Data Release 7 galaxy sample.* Mon. Not. Roy. Astron. Soc. 2010, **401**, pp. 2148 – 2168 (arXiv: 0907.1660)

[10] Kazin E.A. et al. *The Baryonic Acoustic Feature and Large-Scale Clustering in the SDSS LRG Sample.* Astrophys. J. 2010, **710**, pp. 1444 – 1477 (arXiv: 0908.2598)

[11] Blake C. et al. *The WiggleZ dark energy survey: mapping the distance redshift relation with baryon acoustic oscillations.* Mon. Not. Roy. Astron. Soc. 2011, **418**, pp. 1707 – 1724 (arXiv: 1108.2635)

[12] Chuang C-H. et al. *The clustering of galaxies in the SDSS-III Baryon Oscillation Spectroscopic Survey: single-probe measurements and the strong power of $f(z)\sigma_8(z)$ on constraining dark energy.* Mon. Not. Roy. Astron. Soc. 2013, **433**, pp. 3559 – 3571 (arXiv: 1303.4486)

[13] Anderson L. et al., *The clustering of galaxies in the SDSS-III Baryon Oscillation Spectroscopic Survey: Baryon Acoustic Oscillations in the Data Release 10 and 11 Galaxy Samples.* Mon. Not. Roy. Astron. Soc. 2014, **441**, pp. 24 (arXiv: 1312.4877)

[14] Ross A.J. et al., *The Clustering of the SDSS DR7 Main Galaxy Sample I: A 4 per cent Distance Measure at* $z = 0.15$, 2014, 13 pp., (arXiv: 1409.3242)

[15] Simon J., Verde L. and Jimenez R. *Constraints on the redshift dependence of the dark energy potential.* Phys. Rev. D 2005, **71**, 123001 (astro-ph/0412269)

[16] Stern D., Jimenez R., Verde L., Kamionkowski M. and Stanford S. A. *Cosmic chronometers: constraining the equation of state of dark energy. I: $H(z)$ measurements.* J. of Cosmology and Astropart. Phys. 2010, **02**, 008 (arXiv: 0907.3149)

[17] Moresco M. et al. *Improved constraints on the expansion rate of the Universe up to z 1.1 from the spectroscopic evolution of cosmic chronometers.* J. of Cosmology and Astropart. Phys. 2012, **8**, 006 (arXiv: 1201.3609)

[18] Blake C. et al. *The WiggleZ Dark Energy Survey: Joint measurements of the expansion and growth history at* $z < 1$. Mon. Not. Roy. Astron. Soc. 2012, **425**, pp. 405 – 414 (arXiv: 1204.3674)

[19] Zhang C. et al. *Four New Observational H(z) Data From Luminous Red Galaxies Sloan Digital Sky Survey Data Release Seven.* Research in Astron. and Astrop. 2014, **14**, 1221-1233 (arXiv: 1207.4541)

[20] Busca N.G. et al. *Baryon Acoustic Oscillations in the Lyα forest of BOSS quasars.* Astron. and Astrop. 2013, **552**, A96, 18pp. (arXiv: 1211.2616)

[21] Chuang C.H. and Wang Y. *Modeling the Anisotropic Two-Point Galaxy Correlation Function on Small Scales and Improved Measurements of $H(z)$, $D_A(z)$, and $f(z)\sigma_8(z)$ from the Sloan Digital Sky Survey DR7 Luminous Red Galaxies.* Mon. Not. Roy. Astron. Soc. 2013, **435**, pp. 255 – 262 (arXiv: 1209.0210)

[22] Gaztañaga E., Cabre A., Hui L. *Clustering of Luminous Red Galaxies IV: Baryon Acoustic Peak in the Line-of-Sight Direction and a Direct Measurement of $H(z)$.* Mon. Not. Roy. Astron. Soc. 2009, **399**, pp. 1663 – 1680 (arXiv: 0807.3551)

[23] Anderson L. et al. *The clustering of galaxies in the SDSS-III Baryon Oscillation Spectroscopic Survey: Measuring D_A and H at $z = 0.57$ from the Baryon Acoustic Peak in the Data Release 9 Spectroscopic Galaxy Sample.* Mon. Not. Roy. Astron. Soc. 2014, **439**, pp. 83 – 101 (arXiv: 1303.4666)

[24] Oka A. et al. *Simultaneous constraints on the growth of structure and cosmic expansion from the multipole power spectra of the SDSS DR7 LRG sample.* Mon. Not. Roy. Astron. Soc. 2014, **439** pp. 2515 – 2530 (arXiv: 1310.2820)

[25] Font-Ribera A. et al. *Quasar-Lyman α Forest Cross-Correlation from BOSS DR11: Baryon Acoustic Oscillations.* J. of Cosmology and Astroparticle Phys. 2014, **05**, 027 (arXiv: 1311.1767)

[26] Delubac T. et al. *Baryon Acoustic Oscillations in the Lyα forest of BOSS DR11 quasars.* 2014, 17 pp., arXiv: 1404.1801

[27] Clifton T., Ferreira P.G., A. Padilla and Skordis C. *Modified Gravity and Cosmology.* Physics Reports 2012, **513**, pp. 1 – 189 (arXiv: 1106.2476)

[28] Bamba K., Capozziello S., Nojiri S. and Odintsov S.D. *Dark energy cosmology: the equivalent description via different theoretical models and cosmography tests.* Astrophys. and Space Science 2012, **342**, pp. 155 – 228 (arXiv: 1205.3421)

[29] Nojiri S. and Odintsov S.D. *Unified cosmic history in modified gravity: from F(R) theory to Lorentz non-invariant models.* Phys. Rept. 2011, **505**, pp. 59 – 144 (arXiv: 1011.0544)

[30] Pahwa I., Choudhury D. and Seshadri T. R. *Late-time acceleration in Higher Dimensional Cosmology.* J. of Cosmology and Astroparticle Phys. 2011, **09**, 015 (arXiv: 1104.1925)

[31] Grigorieva O.A. and Sharov G.S. *Multidimensional gravitational model with anisotropic pressure.* Intern. Journal of Modern Physics D 2013, **22**, 1350075 (arXiv: 1211.4992)

[32] Sharov G.S. and Vorontsova E.G. *Parameters of cosmological models and recent astronomical observations.* J. of Cosmology and Astroparticle Phys. 2014, **10**, 057 (arXiv: 1407.5405)

[33] Riess A.G. et al. *A 3% Solution: Determination of the Hubble Constant with the Hubble Space Telescope and Wide Field Camera 3.* Astrophys. J. 2011, **730**, 119, 18 pp. (arXiv: 1103.2976)

[34] Kowalski M. et al. *Improved cosmological constraints from new, old and combined supernova datasets.* Astrophys. J. 2008, **686**, pp. 749 – 778 (arXiv: 0804.4142)

[35] Shi K., Huang Y.F. and Lu T. *A comprehensive comparison of cosmological models from the latest observational data.* Monthly Notices Roy. Astronom. Soc. 2012, **426**, pp. 2452 – 2562 (arXiv: 1207.5875)

[36] Farooq O., Mania D. and Ratra B. *Hubble parameter measurement constraints on dark energy.* Astrophys. J. 2013, **764**, 138, 13 pp. (arXiv: 1211.4253)

[37] Farooq O. and Ratra B. *Hubble parameter measurement constraints on the cosmological deceleration-acceleration transition redshift.* Astrophys. J. 2013, **766**, L7, 4pp. (arXiv: 1301.5243)